NANO LETTERS

Letter

pubs.acs.org/NanoLett

Observation of Charge Generation and Transfer during CVD Growth of Carbon Nanotubes

Jiangtao Wang,[†] Peng Liu,[*,†] Bingyu Xia,[†] Haoming Wei,[†] Yang Wei,[†] Yang Wu,[†] Kai Liu,[‡] Lina Zhang,[†] Jiaping Wang,[†,§] Qunqing Li,[†,§] Shoushan Fan,[†,§] and Kaili Jiang[*,†,§]

[†]State Key Laboratory of Low-Dimensional Quantum Physics, Department of Physics & Tsinghua-Foxconn Nanotechnology Research Center, Tsinghua University, Beijing 100084, China

[‡]State Key Laboratory of New Ceramics and Fine Processing, School of Materials Science and Engineering, Tsinghua University, Beijing 100084, China

[§]Collaborative Innovation Center of Quantum Matter, Beijing 100084, China

Supporting Information

ABSTRACT: Carbon nanotube (CNT) is believed to be the most promising material for next generation IC industries with the prerequisite of chirality specific growth. For various approaches to controlling the chiral indices of CNTs, the key is to deepen the understanding of the catalytic growth mechanism in chemical vapor deposition (CVD). Here we show our discovery that the as-grown CNTs are all negatively charged after Fe-catalyzed CVD process. The extra electrons come from the charge generation and transfer during the growth of CNTs, which indicates that an electrochemical process happens in the surface reaction step. We then designed an in situ measurement equipment, verifying that the CVD growth of CNTs can be regarded as a primary battery system. Furthermore, we found that the variation of the Fermi level in Fe catalysts have a significant impact on the chirality of CNTs when different external electric fields are applied. These findings not only provide a new perspective on the growth of CNTs but also open up new possibilities for controlling the growth of CNTs by electrochemical methods.

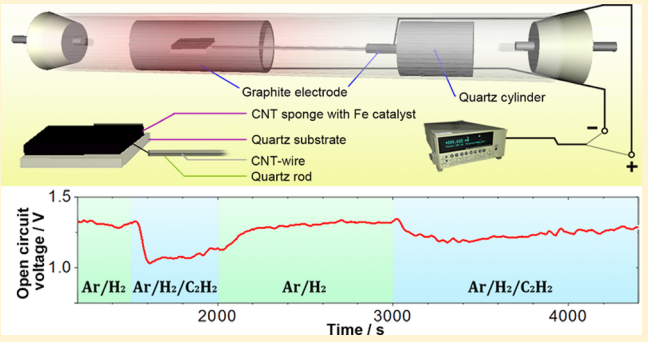

KEYWORDS: *Chemical vapor deposition, growth of carbon nanotubes, negatively charged, electrochemical process, controlled growth*

In recent years, some fantastic carbon nanotube (CNT) based devices have been created successively,[1−5] which implies a bright future of CNT electronics[6] and arouses the desire for direct growth of identical semiconducting CNTs to meet the semiconductor industry standard.[7] For various approaches to controlling the chirality of CNTs,[8−12] the key is to deepen the understanding of the catalytic growth mechanism in chemical vapor deposition (CVD).[13−15] A physical picture focused on carbon atoms transfer in CVD growth of CNTs has been established for two decades.[16−18] However, the charge transfer in the growth process has yet to be systematically studied.

Around the year of 2008, we found that individual ultralong CNTs on a SiO_2/Si substrate could be directly "seen" by using an optical microscope after being exposed to air for a long time (Figure S1a). It did not attract much attention of us until Sep. 2013 when we found that the ultralong CNTs could be "seen" with much shorter time exposed to the air if a substrate coated with alumina was used. The contrast of the ultralong CNTs' image became higher and higher with time. Apparently, CNTs attracted more ambient particles from the surroundings than the substrate did to make themselves visible under an optical microscope (Figure S1b). Intuitively, we speculated that the as-grown CNTs are not electrically neutral. From that time on, some special techniques were invented to verify this speculation.

Because of extremely small capacitance of an individual CNT, any contact measurement of the charge is not feasible. To measure the charge distribution on CNTs, we invent a noncontact technique for direct visualization of surface charge distribution, which is extended from vapor-condensation-assisted (VCA) optical microscopy[19] and is named as e-VCA technique. Briefly, the measurement comprises two steps as shown in Figure 1a. The first step is to spray negatively charged glucose nanoparticles to the sample for about 20 s. The negatively charged nanoparticles will aggregate mostly at positively charged area and avoid depositing on negatively charged area because of Coulomb interaction. Thus, the surface charge distribution will be delineated by glucose nanoparticles, but at this step they are still not visible under an optical

Received: February 26, 2016
Revised: May 17, 2016
Published: June 2, 2016

DOI: 10.1021/acs.nanolett.6b00841
Nano Lett. 2016, 16, 4102−4109

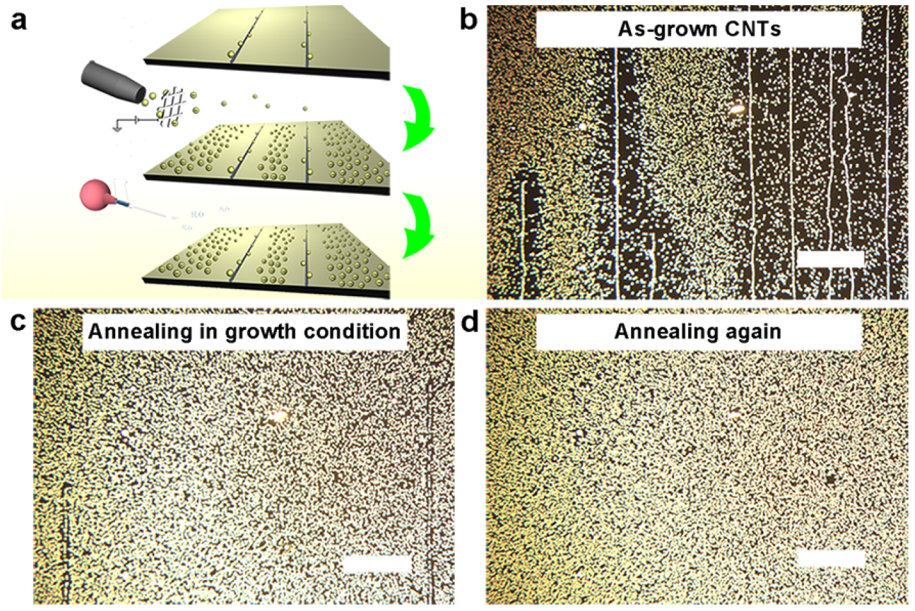

Figure 1. e-VCA imaging of negatively charged as-grown ultralong CNTs. (a) The operation of e-VCA imaging, spraying negatively charged nanoparticles and then blowing warm water vapor to the as-grown ultralong CNTs, which is used to visualize the surface charge distribution along the CNTs. The e-VCA images of as-grown CNTs (b), CNTs annealed in the growth ambient and temperature for 3 min (c), and CNTs annealed again (d) are shown, respectively. Scale bars in b–d are 250 μm.

microscope. The second step is to use VCA optical microscopy to visualize the hydrophilic glucose nanoparticles.[19] The reliability of e-VCA technique is discussed in Supporting Information. With this technique, the charge distribution of ultralong CNTs can be easily and reliably obtained within 1 min.

The ultralong CNTs used in this work were grown by Fe-catalyzed CVD similar to our previous work.[20] Quartz with 0.2-nm-thick Fe and silicon coated with 1-μm-thick silica were used as the catalyst substrate and the receiving substrate, respectively, in order to avoid discharging. Figure 1b shows an e-VCA image of as-grown ultralong CNTs, in which all the ultralong CNTs appear as bright lines surrounded by dark edges. The bright lines originate from the native impurities along CNTs, which are hydrophilic sites generated during the growth process,[19] and the dark edges result from the negative charge distribution along CNTs. For native-impurity-free CNTs, they will be delineated only by dark edges in e-VCA image (Figure S2). It is evident that the as-grown CNTs are negatively charged. To exclude any artificial influence by our operation, we put the specimen back to the furnace and annealed it in the growth ambient and temperature for 3 min with identical tools and operation as the first growth process used. After that, most of CNTs become invisible in the e-VCA image, except two CNTs with much narrower dark edges (Figure 1c). Further, we put the specimen back to the furnace and annealed it in the same condition for another 3 min. After that, nothing is visible in the e-VCA image (Figure 1d). It is obvious that the annealing process leads to discharge of CNTs. The difference in the three e-VCA images should be attributed to the different activity of the catalysts, which are active in growth process and inactive during annealing process. Therefore, these annealing experiments indicate that the charge generation is related to the catalytic growth of CNTs.

As we know, CNTs are classified into semiconducting CNTs (s-CNTs) and metallic or quasi-metallic CNTs (m-CNTs) by their chiral indices. What puzzles us is where the extra electrons are accommodated in the CNTs just after growth? For m-CNTs, extra electrons may be directly filled in their conduction band and the Fermi level will be raised consequently. However, for s-CNTs with bandgap, where are extra electrons filled? To answer this question, we take the following discharging experiments as shown in Figure 2. First, we take e-VCA images for two groups of as-grown CNTs (not discharged) (Figure 2a, b). After using a droplet of deionized water to contact the bottom of the as-grown CNTs (termed as "point-contact") (Figure 2e, f), we take e-VCA images for these two specimens again (Figure 2i, j). By comparing Figure 2a with 2i, we find that the negatively charged as-grown CNTs become discharged, which indicates that the electrons are able to move freely in this type of CNTs. They should be metallic and have been further verified by electrical transport measurements (Figure S3a). Figure 2m illustrates the change of the Fermi level from higher position to neutral position in this discharging process. On the other hand, by comparing Figure 2b with j, the heavily negatively charged as-grown CNTs become slightly negatively charged after the point-contact discharging. We speculate that there are two kinds of electrons in this type of CNTs: one is extended electron filled in the conduction band, and the other is localized electron filled in the impurity level. This type of CNTs should be semiconducting which is also verified by electrical transport measurements (Figure S3b). Figure 2n illustrates that the point-contact discharging operation to these as-grown s-CNTs will exhaust the extended electrons in the conduction band but has no impact on the localized electrons in the impurity level.[21] To confirm this model, we take an e-VCA image of one s-CNT after point-contact discharging (Figure 2c). Then a drop of clean water is placed on the lower part of the s-CNT for 20 s and then is blown away (termed as "surface-contact", Figure 2g). Next, we take the e-VCA image again of this specimen (Figure 2k). Compared with Figure 2c, the lower part is almost electrically neutral, although the upper part of the CNT is still negatively charged. This phenomenon indicates that the localized electrons can be discharged by

DOI: 10.1021/acs.nanolett.6b00841
Nano Lett. 2016, 16, 4102–4109

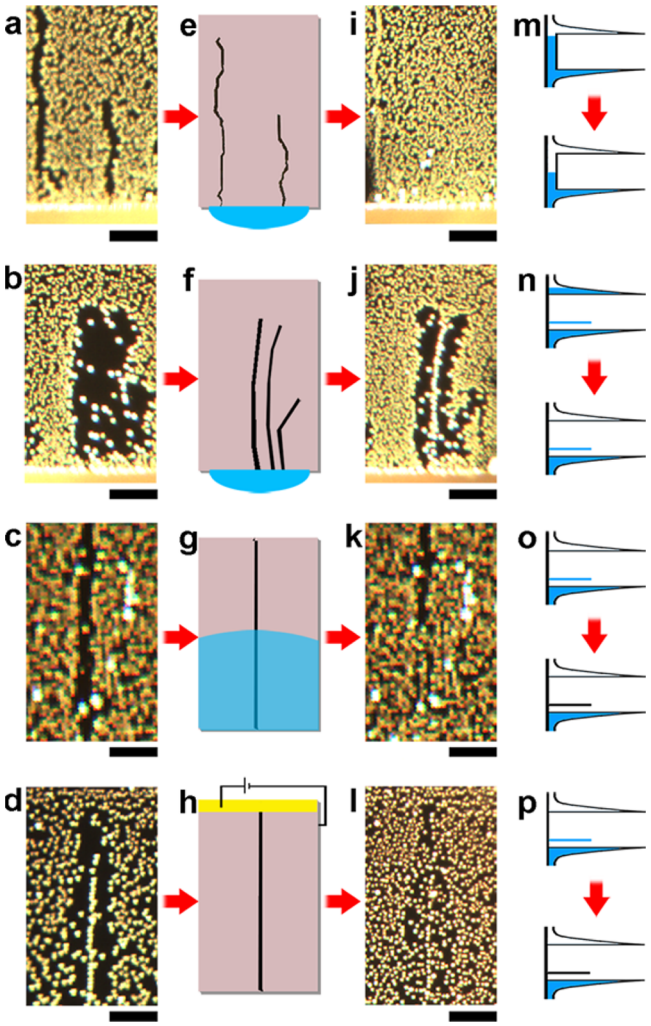

Figure 2. Discharging experiments for studying electron filling in as-grown ultralong CNTs. The e-VCA images of as-grown m-CNTs (a), as-grown s-CNTs (b), and partially discharged s-CNTs (c and d). After the discharge operation (e–h, blue parts represent water), panels i–l show the e-VAC images of the four specimens, respectively. (m–p) The occupied electronic state of ultralong CNTs before and after corresponding discharge operation. Scale bars in (a–d, i–l) are 50 μm.

surface-contact (Figure 2o). Furthermore, we use a CNT film electrode[22] to apply a gate voltage (Figure 2h) to another partially discharged s-CNT. Figure 2d and l show the e-VCA image when the gate voltage is 0 V and −10 V. It can be seen that the entire s-CNT becomes electrically neutral after −10 V gate voltage applied. Because s-CNTs in the ambient air are usually p-type,[21] negative gate voltage will generate holes on the top of the valence band, then the localized electrons in the impurity level will recombine with the holes (Figure 2p). These observations indicate that (1) for as-grown m-CNTs, the extra electrons are accommodated in the conduction band; (2) for as-grown s-CNTs, the extra electrons are accommodated both in the conduction band and the impurity level. It is worth noting that the Fermi level of an isolated s-CNT is difficult to be manually raised to the conduction band in the ambient air. From aforementioned analysis, we propose that an electrochemical process or a primary battery system exists in the CVD growth of CNTs and the electromotive force might be significant.

For a primary battery, it is necessary to measure the open circuit voltage and short circuit current. Figure 3a schematically illustrates the in situ measurement system, including a suspended working electrode and a coaxial graphite counter electrode. The inset shows a high magnification view of the CNT sponge[23] with Fe catalysts at the tip of the working electrode. Figure 3b (and Figure S4) shows the variation of open circuit voltage with feed gas at 700 °C. We find that the open circuit voltage is stable in an atmosphere of 400 sccm Ar and 200 sccm H_2. This background voltage comes from the heating voltage and the temperature difference between graphite tube and the CNT sponge (see Figure S4a and further discussion in Supporting Information). As we add 5 sccm C_2H_2 (the change of the flow rate is less than 1%) to the feed gas, the potential difference drops down by about 0.32 V within 50 s. Based on the variation of the growth rate of CNTs measured by thermal gravimetric analysis (TGA) in the previous work,[24] this period should correspond to the nucleation of CNTs. Then, the open circuit voltage raises back slowly, which corresponds to a gradual deactivation of Fe catalysts. When the C_2H_2 is switched off, the voltage raises back to the background value quickly, which corresponds to a discharge process due to the halt of the growth. Then we add 5 sccm C_2H_2 to the feed gas again. The voltage falls off by only 0.1 V, following which it raises back gradually until equals to the background voltage. These observations indicate that only if the catalysts are active, the electromotive force is obvious. In another measurement, the variation of short circuit current with the feed gas is also recorded (Figure 3c, Figure S4b), showing a similar result to that of open circuit voltage.

To illustrate the gas phase electrochemical process, we suggest a model based on resonant tunneling theory. As shown in Figure 4a, the carbanions are generated when C_2H_2 molecule is adsorbed and cracked by Fe nanoparticles.[25,26] The electrons in high-energy-level C_2H^- carbanions (−2.97 eV)[27] will transfer to low-energy-level Fe catalyst[28] first, resulting in the accumulation of electrons in CNTs. The Fermi level in the catalyst as well as CNT will then be raised up accordingly due to their small quantum capacitance. Meanwhile, H^+ ions generated nearby the surface of Fe catalyst will capture the electrons from the catalyst through tunneling, leading to a decrease of the Fermi level in CNT.[29−32] However, the tunneling probability is negligible if the energy alignment do not meet the resonant condition. Therefore, some of H^+ ions will carry away positive charge with gas flow inducing negative charge accumulation on CNT. Finally, an equilibrium will be established when the flux of electron generation is equal to the flux of tunneling, and the electromotive force $\mathcal{E}$ should equal to the difference between the raised Fermi level and the original Fermi level. Obviously, the anode should be the Fe catalyst, and the cathode is the graphite tube which is used as a counter electrode. The electrochemical reaction happening at anode is

$$2C_2H^- \rightarrow 2C_2H + 2e^- \quad (1)$$

and at cathode is

$$2H^+ + 2e^- \rightarrow H_2 \quad (2)$$

where the H^+ ions are generated from the surface catalytic reaction, and C_2H is the precursor to grow CNTs as the following

$$2C_2H \rightarrow 4C + H_2 \quad (3)$$

DOI: 10.1021/acs.nanolett.6b00841
Nano Lett. 2016, 16, 4102−4109

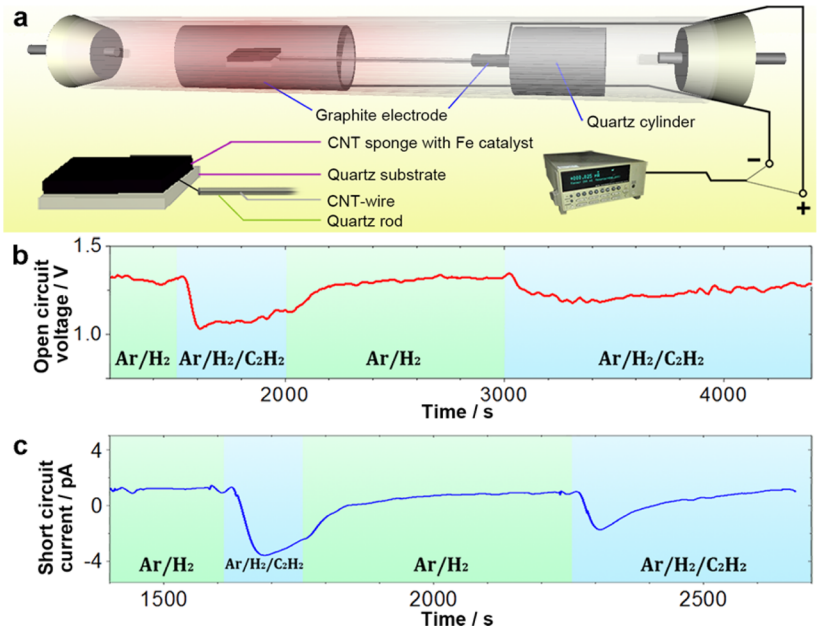

Figure 3. In situ electric measurement for CVD growth of CNTs. (a) The in situ measurement system. The change of open circuit voltage (b) and short circuit current (c) with feed gas.

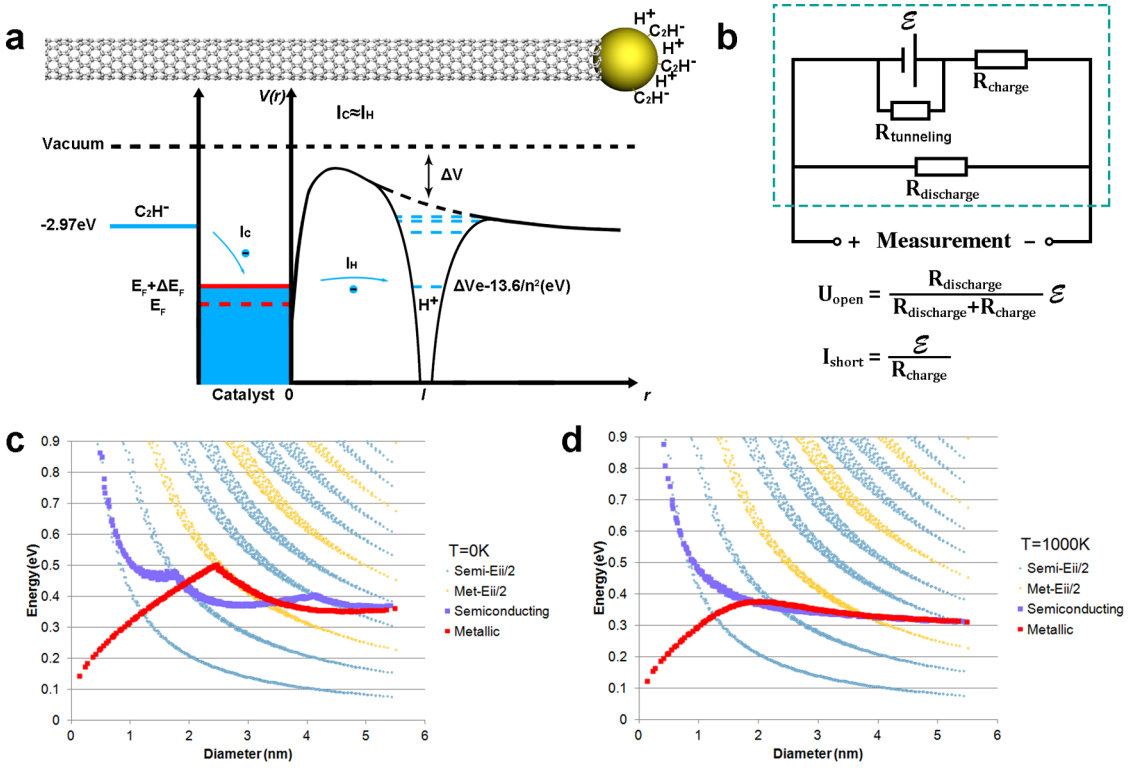

Figure 4. Proposed model for charge generation and transfer. (a) Diagram of electrons transferring among C_2H^-, Fe catalyst, and H^+ during growth of CNTs. (b) The equivalent circuit of the in situ measurement system. U_{open} is the measured open circuit voltage, I_{short} is the measured short circuit current, R_{charge} represents the equivalent resistance of electrons injecting into Fe catalysts, $R_{discharge}$ represents the equivalent resistance of electrons discharging from as-grown CNTs and the CNT sponge, and $R_{tunneling}$ represents the equivalent resistance of electrons tunneling. The calculated Fermi levels of the growing metallic (red) and semiconducting (purple) CNTs at the growth temperature of nearly 0 K (c) and 1000 K (d). The Kataura plot is also presented for comparison.

To further understand the open circuit voltage that we measured, an equivalent circuit for in situ measurement is proposed as shown in Figure 4b. By considering the electrons discharging from the CNT sponge, the real electromotive force $\mathcal{E}$ should be written as

$$\mathcal{E} = \frac{R_{charge} + R_{discharge}}{R_{discharge}} U_{open} \quad (4)$$

where U_{open} is the measured open circuit voltage, R_{charge} represents the equivalent resistance of electrons injecting into

DOI: 10.1021/acs.nanolett.6b00841
Nano Lett. 2016, 16, 4102–4109

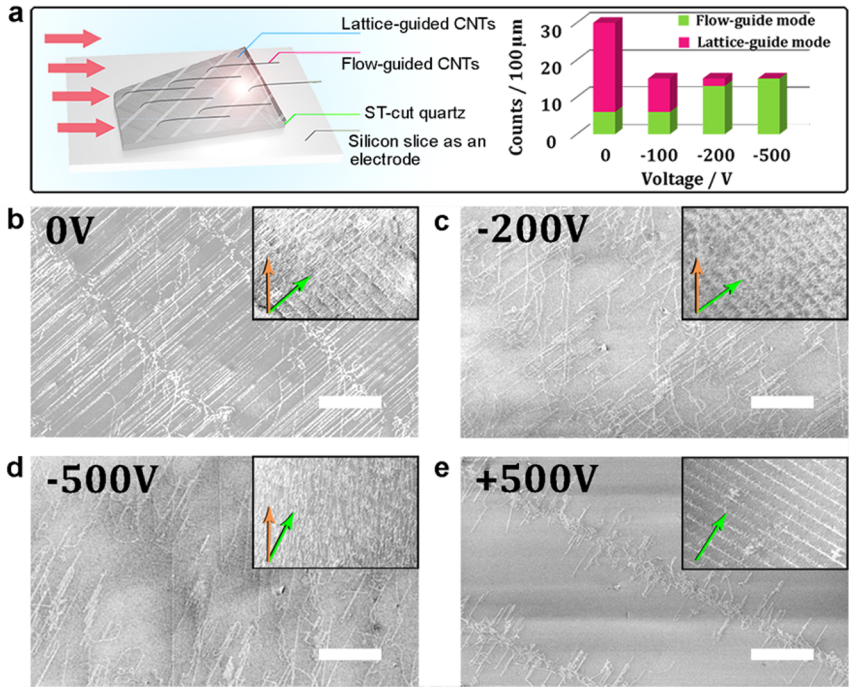

Figure 5. Growth mode controlled by external electric field. (a) Different growth modes are obtained by applying various voltages. SEM image of CNTs grown with 0 V (b), −200 V (c), −500 V (d), and +500 V (e) applied. The insets are the corresponding low magnification views. The red arrows indicate the direction of the flow and the green arrows indicate the direction of the lattice. Scale bars in b−e are 50 μm.

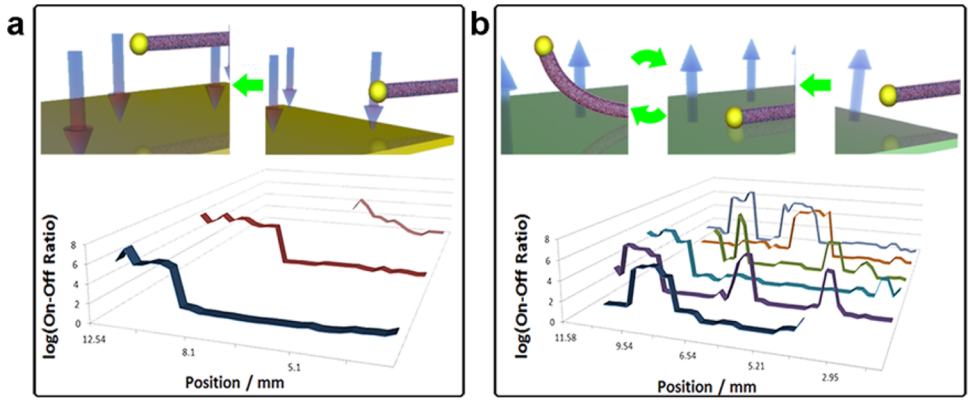

Figure 6. Chirality change of ultralong CNTs during growth on charged substrates. The chirality change of ultralong CNTs grown on negatively charged Si_xN_y surface (a) and positively charged Al_2O_3 surface (b) with the same catalysts. The upper part is the diagrams of the variation of growth mode, and the lower part shows the measured logarithm on−off ratio along the CNTs.

Fe catalysts, and $R_{discharge}$ represents the equivalent resistance of electrons discharging from as-grown CNTs and the CNT sponge. It is evident that larger amount of active Fe catalysts will lead to smaller R_{charge}, and the measured value may be more close to the real electromotive force.

A rough estimation about the increase of the Fermi level can be made by considering the aforementioned equilibrium. The detailed calculation is discussed in Supporting Information. Here we just present the most important results and findings. For a triple-walled CNT with the chiral indices (21, 19), (30, 23), and (33, 31) growing at 700 °C, the growth rate is about 1 μm/s. According to our theoretical analysis (see Supporting Information), the calculated electromotive force is about 0.32 V. For single-walled CNTs, such as (12, 7), growing at 970 °C, the growth rate is nearly 100 μm/s. In this case, the calculated electromotive force is about 0.42 V. It is worth noting that when the CNTs are removed from the growth environment, the negative charge on CNTs will generate much higher electric potential due to the extremely small capacitance between CNTs and the ground.

Furthermore, as presenting the calculated Fermi levels of growing CNTs on Kataura plot (Figure 4c, d),[33] we found that the Fermi levels of s-CNTs are significantly different from that of m-CNTs. It is interesting that the difference between the Fermi levels of s-CNTs and m-CNTs are not monotone with the diameter. Below 2 nm, the Fermi levels of s-CNTs are higher; however, from 2 to 3.5 nm, the Fermi levels of m-CNTs are higher. We believe that this oscillation will have remarkable impact on the diameter-specific growth of s-CNTs.[34,35]

The electron accumulation in the CVD growth of CNTs implies a possibility of controlling the growth of CNTs by using an external electric field. For CNTs growing on single crystal quartz, lattice-guide growth mode is dominant.[36,37] We put a piece of quartz directly on a conducting silicon slice which is

DOI: 10.1021/acs.nanolett.6b00841
Nano Lett. 2016, 16, 4102−4109

used as an electrode. As various voltages applied on the electrode, different proportion of flow-guide mode CNTs are obtained (Figure 5a). With higher negative voltage applied, more CNTs follow the flow-guide growth mode (Figure 5b–d). On the contrary, no CNT takes off from the quartz when positive voltage is applied (Figure 5e). Apparently, the growth mode can be easily controlled by applying an external electric field because of the accumulation of electrons in growing CNTs.

Furthermore, the effect of external electric field on the chiral indices of ultralong CNTs was investigated by changing the insulator layer of the silicon substrate from electric neutrally SiO_2 to negatively charged Si_xN_y and positively charged Al_2O_3, respectively (Figure S5). To facilitate the transport measurement, the electrodes are fabricated on the substrate prior to the growth (Figure S6). The on–off ratio of ultralong CNTs on negatively charged Si_xN_y and positively charged Al_2O_3 substrates are measured segment by segment immediately after growth (Figure 6a, b). We found that the CNTs grown on Si_xN_y changed from metallic to semiconducting, but the CNTs grown on Al_2O_3 changed between metallic and semiconducting for several times. By comparing the results, it is obvious that the two kinds of charged substrates have significantly different impacts on the chiral indices of ultralong CNTs. The reason for this difference is not very clear, but we infer that the change of the chiral indices of CNTs may result from the variation of the Fermi level in Fe catalysts during the growth. Based on the calculation of the Fermi level in growing CNTs (Figure 4c), s-CNTs with large bandgap is apt to be charged to a higher value due to its zero density of state below the first van Hove singularity. Therefore, it is possible that a higher Fermi level may correspond to a higher on–off ratio. When negatively charged growing CNTs are lifted up by the negatively charged Si_xN_y, the Fermi level of the CNTs and catalysts may be kept at a higher position, hence, leading to a higher on–off ratio. On the other hand, negatively charged growing CNTs may be attracted by the positively charged Al_2O_3, and the CNTs are tend to be discharged heavily even to become positively charged, which will cause the CNTs to be lifted up and negatively charged again (Figure S7). With this kind of self-oscillation, the Fermi level in the catalysts and the on–off ratio of the CNTs may oscillate together. Although the real control of the chiral indices of CNTs has not been achieved, our discovery offers the prospect of controlling the chiral indices of CNTs by using electrochemical methods.

It is worth noting that the effect of external electric fields on the growth of CNTs has been already discussed in previous literature. Most of the work focused on the electric-field-directed effect for growing CNTs by using DC or AC electric field.[38−49] The reason for the CNTs' orientation was interpreted as the extra charge from the electrodes or the high polarizability of CNTs. However, the charge generation phenomenon during the growth of CNTs has not been noticed.[50−55] Just before submitting this paper, we found Smovzh and colleagues' paper. They also observed that the CNTs were negatively charged during the thermal CVD growth.[56] Here we not only unambiguously observed that the as-grown CNTs are negatively charged but further verified an electrochemical mechanism which brings a new insight on the controlled growth of CNTs.

In summary, we discovered and studied the charge generation and transfer in CVD growth of CNTs, and achieved the control of the growth mode of CNTs. Our discovery implies an electrochemical process in CVD growth of CNTs that enables people to control the chirality of the CNTs by electrochemical methods. We believe that more accurate control for the growth of CNTs, such as chirality-specific growth, will be achieved by using electrochemical methods in the near future. Furthermore, these new findings and new perspective will also have profound impact on the CVD synthesis of a wide spectrum of nanomaterials.

Methods. *Taking e-VCA Images.* To obtain the negatively or positively charged nanoparticles, an atomizer is used to spray saturated glucose ethanol solution through a metal-grid to which a voltage of about −1800 V or +1800 V is applied. After spraying negatively or positively charged nanoparticles to the substrate, hydrophobic mode VCA imaging technique is used to visualize the nanoparticles.[19]

Deposition of 0.2 nm Fe Film. 0.2 nm Fe is deposited on quartz substrate by using an electron-beam evaporator.

Growth of Ultralong CNTs. To grow ultralong CNTs, the furnace temperature is ramped to 970 °C within 20 min in an atmosphere of Ar with a flow rate of 400 sccm, following which 1.0–1.2 sccm C_2H_4 and 200 sccm H_2 are added to initiate the growth. Finally, after growing for 2–10 min, the sample is withdrawn from the high temperature area and cooled down quickly to the room temperature within 8 min.

In Situ Electric Measurement Installation. The catalysts are prepared by dripping about 1 mL mixed ethanol solution of 50 mmol/L $Fe(NO_3)_3$ and 50 mmol/L $Al(NO_3)_3$ on a piece of CNT sponge.[23] A CNT wire[57] with a quartz sheath is used to connect the CNT sponge to a cylindrical graphite electrode electrically and mechanically. A graphite tube is used as the counter electrode, and the CNT sponge is put at the center of the counter electrode. A DC power source is used to heat the furnace to avoid interference from the AC power source. To avoid noise from environment, grounded nickel foil is used to wrap the quartz tube. Similar to conventional electromotive force measurement, compensation method is used to measure the potential difference between the two electrodes by using a source meter unit Keithley 2410 (Figure 3b). Keithley 6517A is also used to directly measure both the open circuit voltage and the short circuit current (Figure 3c and Figure S4).

Silicon Substrate with Si_xN_y or Al_2O_3 Layer. A 50 nm Si_xN_y layer is grown by plasma enhanced CVD on a silicon substrate with 300 nm SiO_2. A 30 nm Al_2O_3 layer is grown by atomic layer deposition (ALD) on a silicon substrate with 300 nm SiO_2.

Super-Aligned CNT Film Electrodes for On–Off Ratio Measurement. A two-layer cross-stacked super-aligned CNT film is placed on the substrate and patterned by lithography and O_2 reactive ion etching (RIE). Prior to the growth of CNTs, annealing in the atmosphere of H_2 at 970 °C is preferred.

Growth of CNTs on Quartz with External Voltage Applied. The growth process is similar to that of the ultralong CNTs. Before introducing the carbon source, the temperature is raised to 970 °C, and an external voltage is applied to the conducting silicon substrate beneath the quartz.

Growth of Ultralong CNTs on Si_xN_y and Al_2O_3. Due to the different nature of Si_xN_y, Al_2O_3 and SiO_2, the flow rate of C_2H_4 is optimized separately (Figure S8). For ultralong CNTs growth on Si_xN_y, the optimized feed gas is 1.20 sccm C_2H_4 with 400 sccm Ar and 200 sccm H_2. For ultralong CNTs growth on Al_2O_3, the optimized feed gas is 1.00 sccm C_2H_4 with 400 sccm Ar and 200 sccm H_2. The growth temperature is 970 °C for both cases.

DOI: 10.1021/acs.nanolett.6b00841
Nano Lett. 2016, 16, 4102−4109

■ ASSOCIATED CONTENT

Supporting Information

The Supporting Information is available free of charge on the ACS Publications website at DOI: 10.1021/acs.nanolett.6b00841.

1. Ultralong CNTs appearing automatically on an alumina coated substrate; 2. Reliability of e-VCA imaging technique; 3. e-VCA image of as-grown CNTs without native impurities; 4. Transfer characteristic of ultralong CNTs; 5. Background voltage in the in situ measurement; 6. In situ electric measurement during CVD growth of CNTs; 7. Calculation of the rising of the Fermi level in CNTs; 8. Characterization of static charge stored in different insulate layers; 9. Super-aligned CNT film electrodes for transport measurement; 10. Evidence for the oscillation growth on Al_2O_3; 11. VCA images of as-grown ultralong CNTs on Al_2O_3 and Si_xN_y at the same growth condition (PDF)

■ AUTHOR INFORMATION

Corresponding Authors

*E-mail: PengLiu@tsinghua.edu.cn.
*E-mail: JiangKL@tsinghua.edu.cn.

Author Contributions

J.W., P.L., and K.J. conceived the experiments, analyzed the results, and wrote the manuscript. J.W. constructed the e-VCA imaging system, the in situ measurement system, and the electric transport measurement system and performed the experiments. J.W. and B.X. contributed to the sample growth and fabrication. H.W. offered CNT wire. All authors discussed the results and wrote the paper together.

Notes

The authors declare no competing financial interest.

■ ACKNOWLEDGMENTS

This work was supported by the National Basic Research Program of China (2012CB932301) and NSFC (11274190, 51472141, 51472142, 51532008).

■ REFERENCES

(1) Shulaker, M. M.; Hills, G.; Patil, N.; Wei, H.; Chen, H. Y.; Wong, H. S.; Mitra, S. *Nature* **2013**, *501*, 526−30.
(2) Sun, D.-M.; Timmermans, M. Y.; Tian, Y.; Nasibulin, A. G.; Kauppinen, E. I.; Kishimoto, S.; Mizutani, T.; Ohno, Y. *Nat. Nanotechnol.* **2011**, *6*, 156−161.
(3) Cao, Q.; Han, S. J.; Tersoff, J.; Franklin, A. D.; Zhu, Y.; Zhang, Z.; Tulevski, G. S.; Tang, J.; Haensch, W. *Science* **2015**, *350*, 68−72.
(4) Laird, E. A.; Pei, F.; Kouwenhoven, L. P. *Nat. Nanotechnol.* **2013**, *8*, 565−568.
(5) Javey, A.; Guo, J.; Wang, Q.; Lundstrom, M.; Dai, H. *Nature* **2003**, *424*, 654−7.
(6) Avouris, P.; Chen, Z.; Perebeinos, V. *Nat. Nanotechnol.* **2007**, *2*, 605−15.
(7) De Volder, M. F.; Tawfick, S. H.; Baughman, R. H.; Hart, A. J. *Science* **2013**, *339*, 535−9.
(8) Yang, F.; Wang, X.; Zhang, D.; Yang, J.; Luo, D.; Xu, Z.; Wei, J.; Wang, J. Q.; Xu, Z.; Peng, F.; Li, X.; Li, R.; Li, Y.; Li, M.; Bai, X.; Ding, F.; Li, Y. *Nature* **2014**, *510*, 522−4.
(9) Sanchez-Valencia, J. R.; Dienel, T.; Gröning, O.; Shorubalko, I.; Mueller, A.; Jansen, M.; Amsharov, K.; Ruffieux, P.; Fasel, R. *Nature* **2014**, *512*, 61−4.
(10) Bachilo, S. M.; Balzano, L.; Herrera, J. E.; Pompeo, F.; Resasco, D. E.; Weisman, R. B. *J. Am. Chem. Soc.* **2003**, *125*, 11186−7.
(11) Liu, J.; Wang, C.; Tu, X.; Liu, B.; Chen, L.; Zheng, M.; Zhou, C. *Nat. Commun.* **2012**, *3*, 1199.
(12) Omachi, H.; Nakayama, T.; Takahashi, E.; Segawa, Y.; Itami, K. *Nat. Chem.* **2013**, *5*, 572−576.
(13) Khalilov, U.; Bogaerts, A.; Neyts, E. C. *Nat. Commun.* **2015**, *6*, 10306.
(14) Ding, F.; Harutyunyan, A. R.; Yakobson, B. I. *Proc. Natl. Acad. Sci. U. S. A.* **2009**, *106*, 2506−2509.
(15) Rao, R.; Liptak, D.; Cherukuri, T.; Yakobson, B. I.; Maruyama, B. *Nat. Mater.* **2012**, *11*, 213−216.
(16) Chen, Y.; Zhang, Y.; Hu, Y.; Kang, L.; Zhang, S.; Xie, H.; Liu, D.; Zhao, Q.; Li, Q.; Zhang, J. *Adv. Mater.* **2014**, *26*, 5898−922.
(17) Jourdain, V.; Bichara, C. *Carbon* **2013**, *58*, 2−39.
(18) Jiang, K.; Feng, C.; Liu, K.; Fan, S. *J. Nanosci. Nanotechnol.* **2007**, *7*, 1494−504.
(19) Wang, J.; Li, T.; Xia, B.; Jin, X.; Wei, H.; Wu, W.; Wei, Y.; Wang, J.; Liu, P.; Zhang, L. *Nano Lett.* **2014**, *14*, 3527−3533.
(20) Wang, X.; Li, Q.; Xie, J.; Jin, Z.; Wang, J.; Li, Y.; Jiang, K.; Fan, S. *Nano Lett.* **2009**, *9*, 3137−41.
(21) Kim, W.; Javey, A.; Vermesh, O.; Wang, Q.; Li, Y.; Dai, H. *Nano Lett.* **2003**, *3*, 193−198.
(22) Jiang, K.; Li, Q.; Fan, S. *Nature* **2002**, *419*, 801−801.
(23) Luo, S.; Wang, K.; Wang, J.; Jiang, K.; Li, Q.; Fan, S. *Adv. Mater.* **2012**, *24*, 2294−8.
(24) Feng, X.; Liu, K.; Xie, X.; Zhou, R.; Zhang, L.; Li, Q.; Fan, S.; Jiang, K. *J. Phys. Chem. C* **2009**, *113*, 9623−9631.
(25) Pakiari, A. H.; Mousavi, M. *J. Phys. Chem. A* **2011**, *115*, 11796−11809.
(26) Wang, Y.; Yang, X.; Hu, L.; Li, Y.; Li, J. *Chinese Journal of Catalysis* **2014**, *35*, 462−467.
(27) Ervin, K. M.; Lineberger, W. C. *J. Phys. Chem.* **1991**, *95*, 1167−1177.
(28) Michaelson, H. B. *J. Appl. Phys.* **1977**, *48*, 4729−4733.
(29) Gurney, R. *Proc. R. Soc. London, Ser. A* **1931**, *A134*, 137.
(30) Bockris, J.; Khan, U. *Quantum Electrochemistry*; Plenum Press: New York, 1979.
(31) Fowler, R. H.; Nordheim, L. *Proc. R. Soc. London, Ser. A* **1928**, *119*, 173−181.
(32) Flugge, S., Ed. *Electron-Emission Gas Discharge I; Encyclopedia of Physics, Vol. XXI*; Springer-Verlag: Berlin, 1956.
(33) Kataura, H.; Kumazawa, Y.; Maniwa, Y.; Umezu, I.; Suzuki, S.; Ohtsuka, Y.; Achiba, Y. *Synth. Met.* **1999**, *103*, 2555−2558.
(34) Zhang, S.; Tong, L.; Hu, Y.; Kang, L.; Zhang, J. *J. Am. Chem. Soc.* **2015**, *137*, 8904−7.
(35) Li, J.; Liu, K.; Liang, S.; Zhou, W.; Pierce, M.; Wang, F.; Peng, L.; Liu, J. *ACS Nano* **2014**, *8*, 554−62.
(36) Zhang, B.; Hong, G.; Peng, B.; Zhang, J.; Choi, W.; Kim, J. M.; Choi, J.-Y.; Liu, Z. *J. Phys. Chem. C* **2009**, *113*, 5341−5344.
(37) Ding, L.; Yuan, D.; Liu, J. *J. Am. Chem. Soc.* **2008**, *130*, 5428−9.
(38) Maeda, M.; Kamimura, T.; Matsumoto, K. *Appl. Phys. Lett.* **2007**, *90*, 043119.
(39) Gao, Y.; Zhou, Y. S.; Xiong, W.; Mahjouri-Samani, M.; Mitchell, M.; Lu, Y. F. *Appl. Phys. Lett.* **2009**, *95*, 143117.
(40) Zhang, Y.; Chang, A.; Cao, J.; Wang, Q.; Kim, W.; Li, Y.; Morris, N.; Yenilmez, E.; Kong, J.; Dai, H. *Appl. Phys. Lett.* **2001**, *79*, 3155−3157.
(41) Ural, A.; Li, Y.; Dai, H. *Appl. Phys. Lett.* **2002**, *81*, 3464−3466.
(42) AuBuchon, J. F.; Chen, L.-H.; Gapin, A. I.; Jin, S. *Chem. Vap. Deposition* **2006**, *12*, 370−374.
(43) Dittmer, S.; Svensson, J.; Campbell, E. E. B. *Curr. Appl. Phys.* **2004**, *4*, 595−598.
(44) Hongo, H.; Nihey, F.; Ochiai, Y. *J. Appl. Phys.* **2007**, *101*, 024325.
(45) Nojeh, A.; Ural, A.; Pease, R. F.; Dai, H. *J. Vac. Sci. Technol., B: Microelectron. Process. Phenom.* **2004**, *22*, 3421−3425.
(46) Chiu, C.-C.; Tai, N.-H.; Yeh, M.-K.; Chen, B.-Y.; Tseng, S.-H.; Chang, Y.-H. *J. Cryst. Growth* **2006**, *290*, 171−175.
(47) Plaza, E.; Briceño-Fuenmayor, H.; Arévalo, J.; Atencio, R.; Corredor, L. *J. Nanopart. Res.* **2015**, *17*, 1−11.

DOI: 10.1021/acs.nanolett.6b00841
Nano Lett. 2016, 16, 4102−4109

(48) Matsuda, T.; Mesko, M.; Ishikawa, T.; Sato, J.; Ogino, A.; Tamura, R.; Nagatsu, M. *Jpn. J. Appl. Phys.* **2008**, *47*, 7436.
(49) Bao, Q.; Pan, C. *Nanotechnology* **2006**, *17*, 1016.
(50) Joselevich, E.; Lieber, C. M. *Nano Lett.* **2002**, *2*, 1137−1141.
(51) Peng, B.; Jiang, S.; Zhang, Y.; Zhang, J. *Carbon* **2011**, *49*, 2555−2560.
(52) Jespersen, T. S.; Nygård, J. *Nano Lett.* **2005**, *5*, 1838−41.
(53) Radu, I.; Hanein, Y.; Cobden, D. H. *Nanotechnology* **2004**, *15*, 473.
(54) Yu, Q.; Qin, G.; Li, H.; Xia, Z.; Nian, Y.; Pei, S.-S. *J. Phys. Chem. B* **2006**, *110*, 22676−22680.
(55) Bulgakova, N. M.; Bulgakov, A. V.; Svensson, J.; Campbell, E. E. *Appl. Phys. A: Mater. Sci. Process.* **2006**, *85*, 109−116.
(56) Smovzh, D. V.; Maltsev, V. A.; Dittmer, S.; Zaikovsky, V. I.; Campbell, E. E.; Nerushev, O. A. *Chem. Vap. Deposition* **2010**, *16*, 225−230.
(57) Wei, H.; Wei, Y.; Wu, Y.; Liu, L.; Fan, S.; Jiang, K. *Nano Res.* **2013**, *6*, 208−215.

DOI: 10.1021/acs.nanolett.6b00841
Nano Lett. 2016, 16, 4102−4109